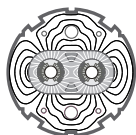EUROPEAN ORGANIZATION FOR NUCLEAR RESEARCH
European Laboratory for Particle Physics

Large Hadron Collider Project

LHC Project Report 500

Proton losses upstream of IP8 in LHC

I. Baishev[*,†], J.B. Jeanneret and K.M. Potter

Abstract

In this report we analyse possible distant sources of proton losses in the long straight section around IP8. These sources can be collisions of the beam protons with nuclei of residual gas in the arcs, betatron cleaning inefficiency and proton-proton collisions in IR1.

[*]Institute for High Energy Physics, Protvino, Russia.
[†]Member of the Russian collaboration to the LHC Project.

1   Introduction

Proton losses upstream of the interaction points can contribute to background in the detectors. The generic losses result from multiple production of secondary particles in inelastic interactions of the beam protons with residual gas nuclei. The distribution of the primary collisions along the machine reflects directly the distribution of the gas density. But the map of impact of secondary particles differs substantially from these two distributions. In particular, elastic and inelastic collisions with at least one energetic proton in the final state result in particle loss far from the point of the primary collision. The first estimations of the losses due to beam-gas scattering in the arcs were given in [1] for IR5. Beam halo tails from the cleaning system and diffractive protons from another IP are listed in [2] among the beam loss sources taken into account in calculations of accelerator related background in the CMS detector. Both studies were made with lattice version 4.1 or earlier. In this work we estimate the proton losses resulting from similar origins for the straight section around IR8 in lattice version 6.1. Specifically, these origins are:

- beam-gas scattering, i.e. collisions of the beam protons with the nuclei of the residual gas in the arc cells and dispersion suppressors;
- collimation inefficiency, i.e. proton out-scattering from the collimators not followed by absorption in the collimators or in other elements of the cleaning system;
- proton-proton collisions in high luminosity interaction points.

2   Reduction of the problem

The neighbouring insertions to IP8 are the betatron cleaning insertion which is upstream of IR8 for Ring 1 and the high luminosity insertion 1 which is upstream of IR8 for Ring 2, see Fig. 1. The effective aperture of the inner triplets in IR1 is approximately 10 r.m.s. beam sizes (10σ) for the nominal value of the betatron function $\beta^* = 0.5$ m at the collision point [6]. The aperture in IR1 will in addition be limited to a similar value in the horizontal plane downstream of the collision point at D2 and Q5 in order to protect the adjacent dispersion suppressor from hard diffractive losses [4],[5]. In IR7, the nominal working position of the primary collimators is at 6σ from the reference trajectory. In IP8 and in the worst case of collision optics with $\beta^* = 1$ m the effective aperture limitation in the triplet is 14σ [7]. Therefore IR1 and IR7 each isolate quite well IR8 from all the distant sources except for those located in arc 7/8 for Ring 1 and sector 8/1 for Ring 2. The optics of IR8 [3],[8] is flexible enough to allow a wide range of β^*, i.e. 1 m $\leq \beta^* \leq 50$ m. The betatron functions in IR8 are shown in Figure 2a for three values of β^*. At $\beta^* = 1$ m the optics of IR8 is similar to the optics of IR1 and IR5 with high beta peaks of 2300 m inside the inner triplet Q1-Q3. The beta peaks do not exceed a few hundred metres for moderate β^* (10-50 m) and these optics are therefore not demanding in terms of aperture in comparison with the optics for $\beta^* = 1$ m. The normalised aperture of IR8 is shown in Figure 2b. Obviously the case of $\beta^* = 1$ m differs from the two others because of the "bottleneck" inside the inner triplet.

3   Simulation

In our simulations we use the version STR00 of the STRUCT code [9]. The original STRUCT code allows for particle tracking in an accelerator lattice with aperture checking for every lattice element. The special features of the STRUCT code include simulation of the proton interaction with collimators or some other scattering elements [10] and the possibility to correctly track protons with momentum p different from the beam
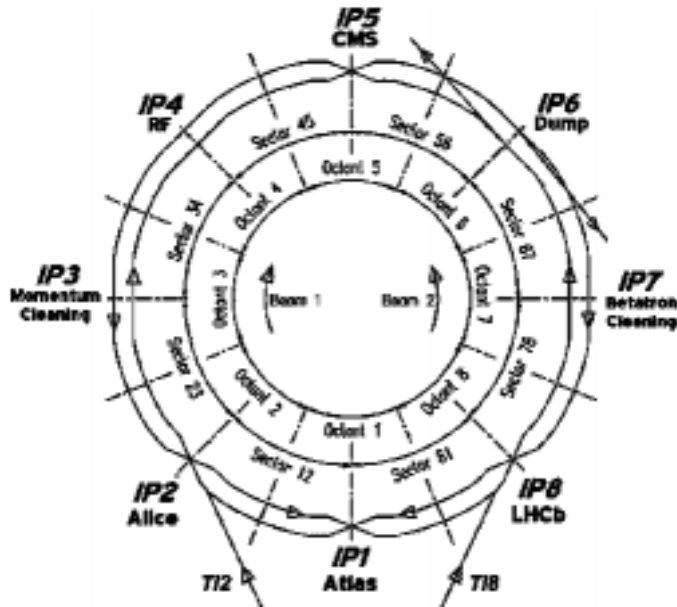
Figure 1: A schematic view of the LHC ring.

momentum p_0 in the range of $\delta_p = 1 - p/p_0 \leq 0.3$. For any particular simulation STRUCT needs some source of the primary particles as input data for tracking. In STR00, the production of secondary particles issued from beam-gas and proton-proton collisions in the range $\delta_p \leq 0.3$ is built-in. A "kicker" is also added to the list of the standard lattice elements for adequate tracking through the insertions with the beam separation/collision elements.

4   Beam-gas collisions

A uniform distribution of the gas density along the arcs and dispersion suppressors is assumed in the simulations though any other reasonable distribution can be taken into account. In the straight section, gas densities are expected to be at least an order of magnitude smaller than in the arcs. Beam-gas scattering is therefore neglected in this area . Following [11],[12] and [13] we consider a gas composition made of hydrogen (20%), carbon (30%) and oxygen (50%) nuclei. In the absence of a firm estimate of absolute residual gas densities, we present results which are normalised to one inelastic interaction per longitudinal metre of the beam protons with the nuclei of residual gas.

Elastic and inelastic collision products in the range $\delta_p \leq 0.3$ are produced all along the arc 7/8 and tracked up to the collision point 8. A map of particles surviving through the arc and impacting onto the wall of the vacuum chamber is shown in Fig. 3. Obviously the optics of IR8 for $\beta^* = 1$ m is significantly more sensitive to the beam losses than those with larger β^*. The "bottleneck" in the inner triplet collects many more protons than the rest of the straight section in that case.

The distribution of the longitudinal coordinate of the production point for protons lost in the straight section is shown in Fig. 4. This demonstrates the ability of the inner triplet to collect scattered protons from the entire arc sector when β^* is small enough. For large β^* the contribution of the protons scattered in distant arc cells is negligible. The structure of the distribution is explained by two facts. To be lost in the triplet where β is large and therefore where the phase advance is very small, a proton must be close to its maximum betatron oscillation. It must therefore be produced at a location which has a
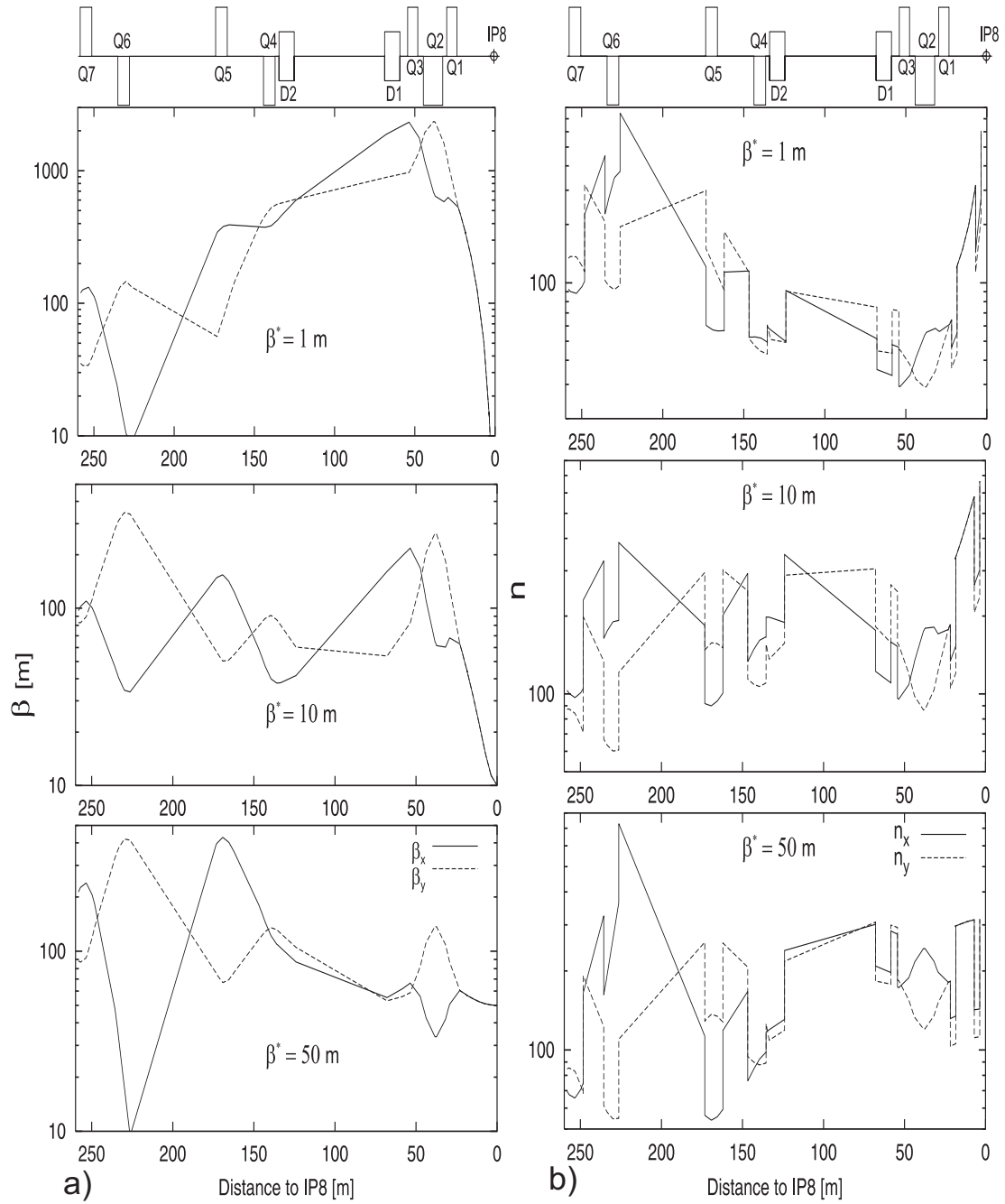
2

Figure 2: The optics on the left half of IR8 (Ring1).On the left side, the beta functions. On the right side, the normalised betatron aperture. From top to bottom, the betatron function at the crossing point is $\beta^* = 1, 10, 50$ m respectively.
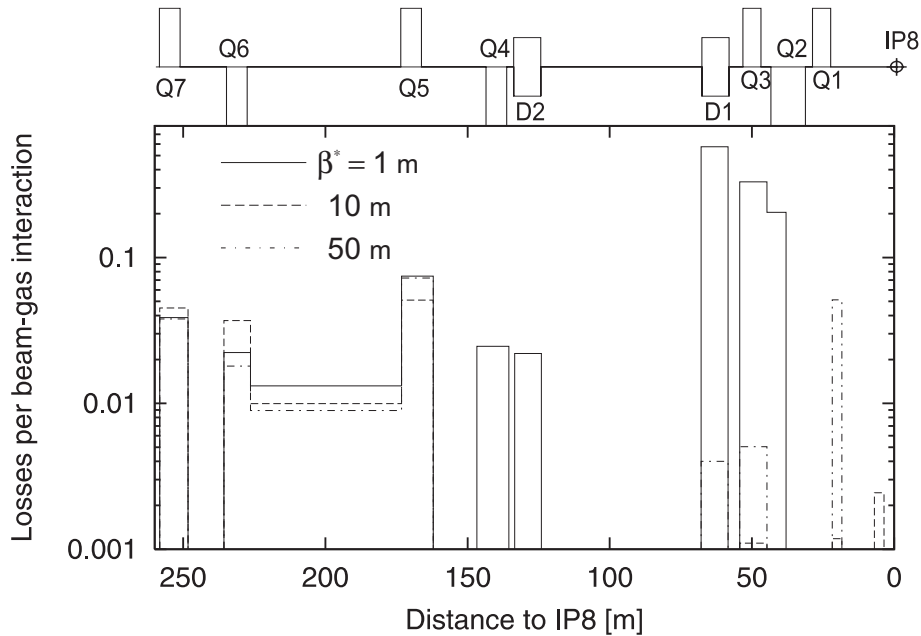
Figure 3: Loss density in IR8 due to the beam-gas scattering in the arc sector 78. Given per unity of linear density of beam-gas inelastic interactions.

phase difference of $\pi/2 + n\pi$ from the triplet. This explains the strong modulation of the distribution. In addition it will be more efficiently collected at an aperture bottleneck if the normalised kick at the production point is large. This condition is met at a location where β is large and therefore where the divergence is small. This explains the secondary modulation of the distribution. This last one is specific to the case studied. It would disappear in a case where locations of maximum β in the arc were in phase with the triplet.

The losses which occur between Q7 and Q5 in Fig. 3 have their origin in the last few hundred meters of the arc and in the close dispersion suppressor (see Fig. 5). These losses are identified with off-momentum protons. This is explained by the fact that these protons are on average produced on the reference orbit where the parent proton has $\delta_p = 0$, while the regular trajectory of off-momentum protons is displaced transversely by $\delta_p \times D$ with D the dispersion at the production point. This results in an effective non-zero dispersion in the straight section, which is larger for larger δ_p.

The rates of losses are similar between Q7 and Q5 for the three cases of β^*. This is explained by the fact that for large δ_p, the effect of the mismatch of dispersion dominates effects related to betatron amplitudes. Protons with large δ_p cannot survive long. This is visible in Fig. 5, where off-momentum protons lost between Q7 and Q5 are almost all produced in the last fifty metres of the arc. The more distantly produced protons, which are lost between Q7 and Q5, have a smaller δ_p and their betatron amplitude is more important, thus explaining why the curve labelled $\beta^* = 50$ m is above the one labelled $\beta^* = 10$ m. In the former case, the normalised betatron aperture of the insertion is smaller in the straight section because of larger β's near Q5 and Q6 as shown in Fig. 2.

The integrated losses along IR8, obtained by integrating the distributions shown in Fig. 3 are given in Table 1. The normalisation is always made for one inelastic interaction per metre of arc.
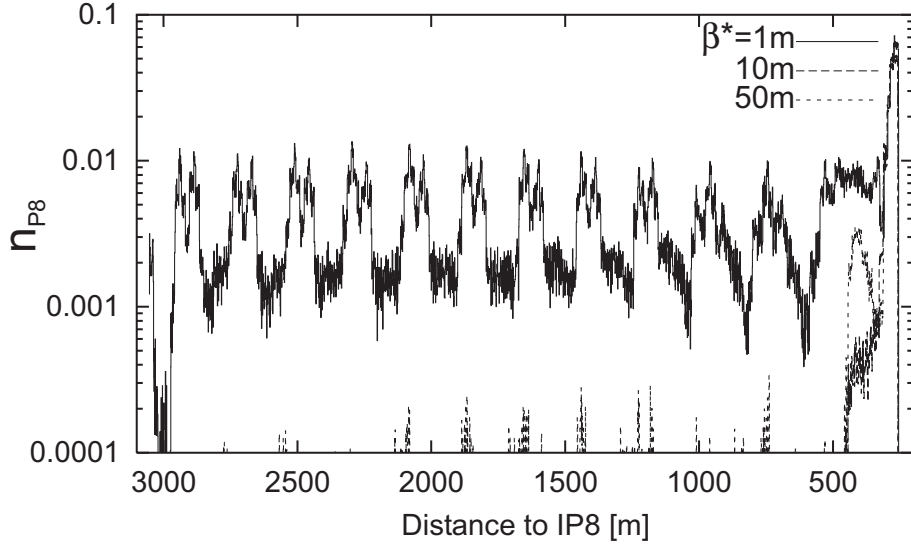
4

Figure 4: The longitudinal distribution of coordinate of beam-gas collisions in the arc sector 7-8 which result in the loss of the scattered proton in the left part of IR8. Normalised to one inelastic interaction per metre of arc.
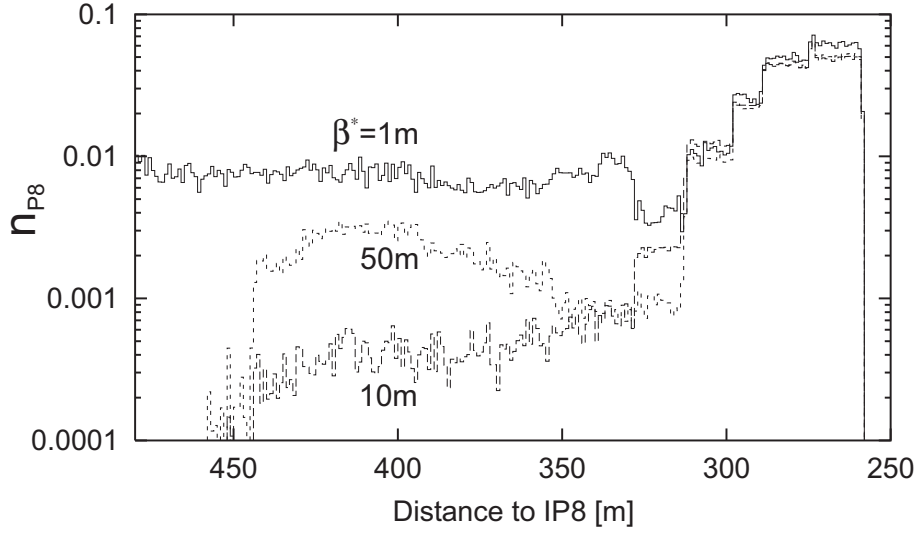

Figure 5: Same as Fig. 4, restricted to the last segment of the arc. The index $1, 10, 50$ m refer to the value of β^*, see text.

Table 1: Integrated losses in IR8, normalised to one inelastic interaction per metre of arc. Otherwise said, with one inelastic interaction per metre of arc, the contribution of the full arc to the total rate of losses in IR8 is the value quoted.

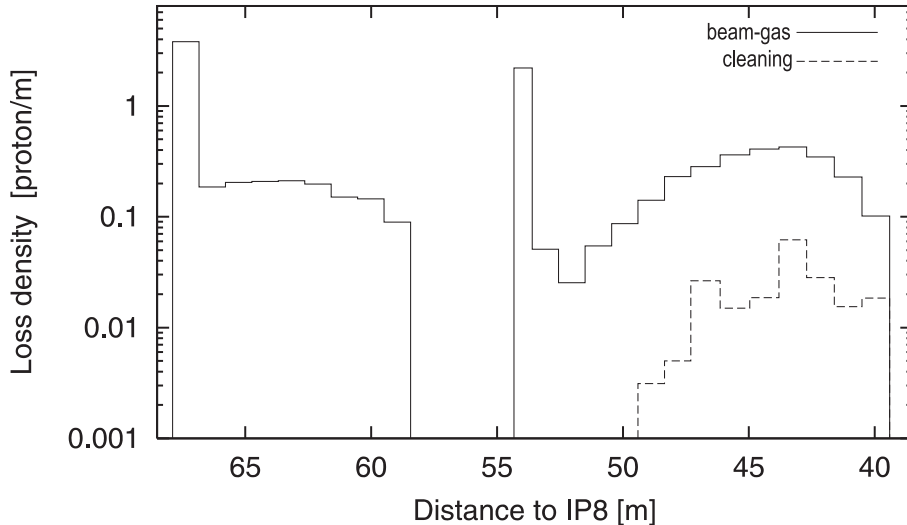| β^* [m]	1	10	50
Losses [m]	12.6	1.92	2.09

Figure 6: Loss density near the D1-Q3-Q2-Q1 low-beta section for $\beta^* = 1$ m. Two origins of the losses are compared : beam-gas scattering in the arc sector 78 (solid histogram) and the betatron cleaning inefficiency (dashed histogram). The first source is given per unity of linear density of beam-gas inelastic interactions. The second one corresponds to 10^5 protons absorbed by the cleaning system.

5   Cleaning inefficiency

The tertiary losses leaving the collimation insertion are simulated with the STRUCT code. A transverse diffusion of the halo with a drift speed of 1 σ/s [14] is simulated first to obtain the map of impacts on the primary collimators. This map is used to simulate the cleaning process including proton scattering in the collimators and multi-turn tracking of the scattered protons with aperture checking for each element of the sector 78 and of IR8.

The losses in IR8 due to cleaning inefficiency amount to $2.2 \cdot 10^{-6}$ protons per one proton absorbed by the cleaning system for $\beta^* = 1$ m. Their distribution normalised to 10^5 protons absorbed by the cleaning system is shown in Figure 6 in comparison with the beam-gas losses discussed in the previous section. In the case of $\beta^* = 10$ m, $3 \cdot 10^7$ primary protons captured by the collimation system resulted in no loss in IR8 in the simulation. We conclude that for $\beta^* \geq 10$ m the contribution of cleaning inefficiency to the losses in IR8 is negligible.

6   Collisions in IP1

Only two kinds of collision products can travel far into the ring, namely those resulting from either elastic or diffractive collisions. Elastic protons are on-momentum and get transverse kicks which are much smaller than the divergence of the beam at the collision point. They therefore remain stable circulating particles. Diffracted protons also get very small normalised transverse kicks, but their momentum offset can be large. Outside the range where the chromatic correction of the ring is good ($|\delta_p| < 3 \times 10^{-3}$), the mismatch of their Twiss functions is important. In particular the dispersion function D can be large at large $|\delta_p|$ even in the straight sections where it is equal to zero for on-momentum protons, thus allowing losses of protons with large momentum offset. The rate of losses in IR8 resulting from IP1 is small and a simplified and efficient procedure can therefore be used to estimate it. We generate protons with δ_p and 4-momentum transfer
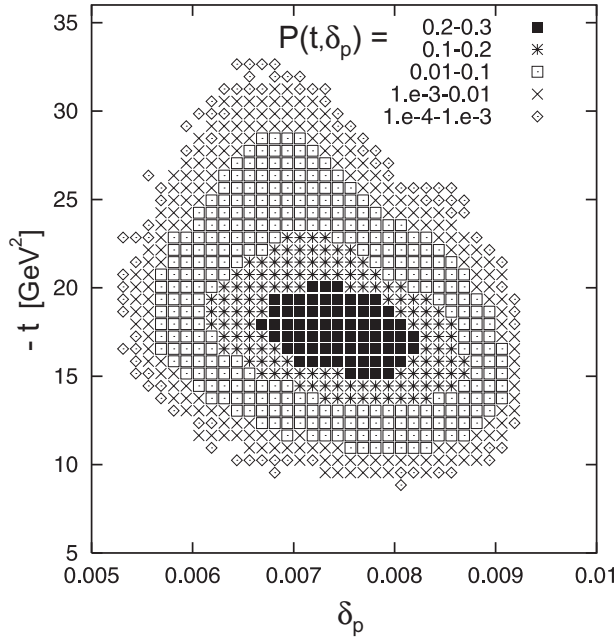
Figure 7: The probability to be lost in IR8 ($\beta^* = 1$ m) for protons scattered in IP1 with the 4-momentum transfer t and the relative momentum loss δ_p generated according to Eq.6.

$|t| = p\theta$, where θ is the scattering angle, from a uniform distribution in the range

$$0 \le |\delta_p| \le 10^{-2} \quad , \quad 0 \le |t| \le 50 \text{ GeV}^2 \ .$$

By tracking through the sector 81 we obtain the probability distribution of losses in IR8. This simulated distribution $P(t, \delta_p)$ is shown in Figure 7 for $\beta^* = 1$ m in IP8. We then integrate the differential cross-section

$$\sigma_{\text{IP1}-\text{IR8}} = \int \int dt d\delta_p \frac{d^2 \sigma_{sd}}{dt d\delta_p} P(t, \delta_p) \ ,$$

of the proton-proton interaction which are in the range of acceptance obtained by the tracking described above, where $\frac{d^2 \sigma_{sd}}{dt d\delta_p}$ is the differential cross-section of proton-proton single diffraction. Using the results of the most recent comprehensive study [15] of single diffraction we obtain a very small effective cross-section $\sigma_{\text{IP1}-\text{IR8}} = 10^{-17}$ mb. The extension to high t [16] of the differential cross-section taken from [15] gives a significantly larger but still small value $\sigma_{\text{IP1}-\text{IR8}} = 8.6 \cdot 10^{-10}$ mb. Multiplying this last value by the nominal luminosity $\mathcal{L} = 10^{34}$ cm^{-2}s^{-1}, we obtain an integral loss rate of $\dot{n}_{\text{IP11}-\text{IR8}} = 10^{-2}$ p/s in IR8 . In the case of $\beta^* \ge 10$ m this rate is smaller by at least a factor 100. The contribution of collisions at point 1 is therefore marginal, when compared to the other contributions discussed above.

7 Approximate absolute rates

We propose the following approximation to obtain an absolute rate in IR8. In the absence of a good a-priori knowledge of the dynamic vacuum pressure in the LHC, and also in the absence of quantified operational scenarios, we use the estimate deduced from [17] for a beam-gas partial lifetime of $\tau_{\text{beam}} = 85$ hrs $= 3.06 \times 10^{15}$ s. With the nominal
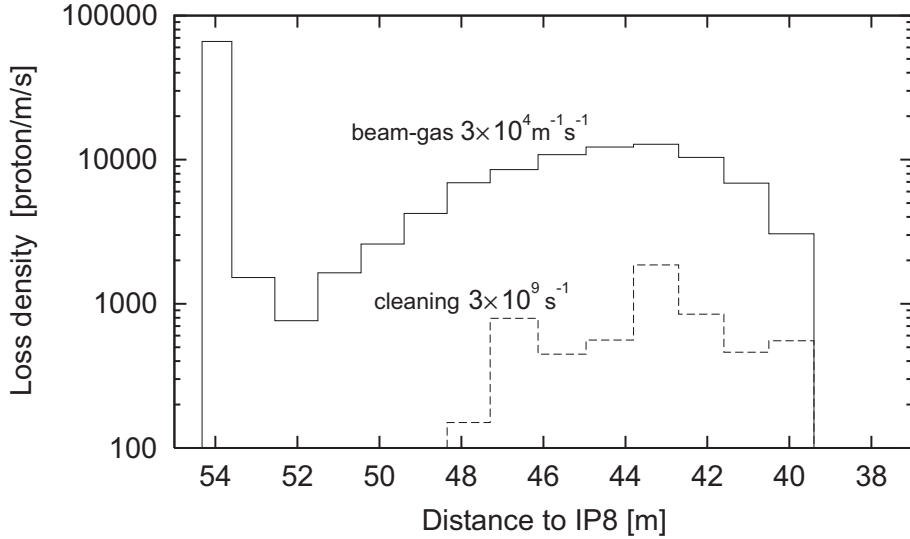
Figure 8: Absolute rates near IP8 for $\beta^* = 1$ m, with the hypotheses discussed in the text. Two sources are considered, namely beam-gas scattering in the arc sector 78 (solid histogram) and tertiary halo protons leaving the betatron collimation insertion (dashed histogram).

stored intensity $N_p = 3 \times 10^{14}$ and the LHC total ring length $L_{\mathrm{ring}} = 26660$ m, the beam gas loss rate per unit length is

$$\dot{n}_{bg} = \frac{N_p}{\tau_{\mathrm{beam}} L_{\mathrm{ring}}} \approx 3 \times 10^4 \text{ p/m/s} . \tag{1}$$

As for the cleaning rate, we use the rate of primary halo $\dot{N} = 3 \times 10^9$ p/s which corresponds to an approximate partial beam life-time of 30 hrs[17]. The normalised distributions of Fig. 6 multiplied by a factor $\dot{n}_{\mathrm{bg}}$ and $\dot{N}$ respectively are shown in Fig. 8 for the final triplet. The tertiary halo from the collimation system (dashed curve) is first corrected by the factor 10^5 used in Fig. 6 for presentation reasons. With the hypotheses made here, the losses related to collimation inefficiency are substantially smaller than the beam-gas interactions. Losses in IR8 which are related to IP1 collision products are marginal. Using the numbers obtained above and the integrated yield given in Table 1 for the beam-gas yield, the integrated absolute rate at point 8 would be

$$\dot{n}_{\mathrm{IR8}} = 12.6 \, \dot{n}_{\mathrm{bg}} + 2.2 \times 10^{-6} \dot{N} = 3.8 \times 10^5 + 7 \times 10^3 \approx 4 \times 10^5 \text{ p/s}$$

In this study a perfectly centred beam was assumed in the triplet of IR8. If the normalised aperture is reduced by 30%, all kinds of losses considered would grow by a factor five.

8   Conclusions

We studied the beam losses in IR8 which are induced by beam-gas scattering, tertiary halo from the betatron collimation insertion and high luminosity collision points. We can summarise our results as follows.

  – Beam-gas scattering is the main distant source of losses in IR8.
  – The contribution of the collimation inefficiency can be significant in the case of extremely low densities of the residual gas along the upstream arc.

8

- The contribution of high luminosity interaction points is negligible.
- By machine symmetry the results of this work obtained for the straight section IR8 are also expected to apply to the straight section IR2.

References

[1] I. Baishev, In: Workshop on LHC Backgrounds, K. Potter ed., March 1996.

[2] A.I. Drozhdin et al., Nucl.Instr.Meth. A381, 531(1996).

[3] O. Bruening, LHC Project Note 193, 1998.

[4] I. Ajguirei, I. Baichev and J.B. Jeanneret, *Beam Losses far downstream of the High Luminosity Interaction Points of LHC*, CERN-LHC-Project-Report-398, CERN, Geneva, August 2000 and EPAC2000, 7th Eur. Part. Acc. Conf., Vienna, Austria, June 2000.

[5] I. Baishev, LHC Project Note 240, November 2000.

[6] O. Bruening, W. Herr and R. Ostojic, LHC Project Report 315, October 1999.

[7] O. Bruening, W. Herr and R. Ostojic, LHC Project Report 367, January 2000.

[8] O. Bruening et al., LHC Project Report 367, 2000

[9] I. Baishev et al., SSCL-MAN-0034, Dallas, 1994

[10] I. Baishev, Preprint IHEP 87-147, Serpukhov, 1987.

[11] A. Mathewson, In: Workshop on LHC Backgrounds, K. Potter ed., March 1996.

[12] O.B. Malyshev and I.R. Collins, Vacuum Technical Note 99-14, 1999.

[13] O.B. Malyshev and A. Rossi, LHC Project Report 437, 2000.

[14] N. Catalan Lasheras et al., LHC Project Report 156, 1997.

[15] K. Goulianos and J. Montanha, Phys.Rev. D59, 114017(1999).

[16] I. Baishev, CERN-SL-2000-077 AP (2000).

[17] The Large Hadron Collider, CERN/AC/95-05(LHC),1995, p. 48.